Eur. Phys. J. B **33**, 31–39 (2003)
DOI: 10.1140/epjb/e2003-00138-y

THE EUROPEAN PHYSICAL JOURNAL B

In situ measurement of high-temperature thermal diffusivity in a combustion-synthesized ceramic

D. Vrel[1,3,a], S. Dubois[2,3], E.M. Heian[2,3], N. Karnatak[2,3], and M.-F. Beaufort[2,3]

[1] Laboratoire d'Ingénierie des Matériaux et des Hautes Pressions[b], 99 avenue J.-B. Clément, 93430 Villetaneuse, France
[2] Laboratoire de Métallurgie Physique[c], bâtiment SP2MI, BP 30179, boulevard M. et P. Curie, 86962 Futuroscope Cedex, France
[3] Groupe Français d'Autocombustion, GDR 2391, J.-C. Niepce, LRRS, BP 47870, 21078 Dijon, France

Received 29 November 2002 / Received in final form 19 March 2003
Published online 23 May 2003 –

Abstract. A simple method to calculate thermal diffusivity *in situ* after a combustion synthesis reaction is presented. The combustion reaction was analyzed *via* time-resolved X-ray diffraction analysis and infrared thermography. Thermal diffusivity was estimated and used to calculate temperature profiles based on temperature profiles one second earlier. For a sample of TiC formed from Ti and C, a value of $2.00 \times 10^{-6} \pm 0.20 \times 10^{-6}$ m^2 s^{-1} was calculated for temperatures between 1000 and 1900 K. This method is rapid and can avoid some problems associated with furnace-based measurements of thermal diffusivity, such as recrystallization and destruction of non-equilibrium phases.

PACS. 44.30.+v Heat flow in porous media – 81.20.Ka Chemical synthesis; combustion synthesis – 61.10.-i X-ray diffraction and scattering

1 Introduction

Self-propagating High-temperature Synthesis (SHS) is a process commonly used on a laboratory scale to produce ceramics and intermetallics, usually from elemental powders. The reaction considered here produces titanium carbide from titanium and graphite powders, according to the reaction Ti + C → TiC. Once ignited at one end of a pre-compacted sample, a reaction front propagates to convert the whole sample into titanium carbide.

Combustion synthesis can produce quite varied results depending on a number of difficult-to-characterize parameters, including reactant particle morphology, size distribution, and ductility; wetting characteristics of the reactants and products; compact density; and density gradients within a compact created by uniaxial pressing. The ability to characterize the thermal diffusivity of a particular sample after the reaction will help to elucidate the effects of these different parameters on the reaction characteristics. In addition, thermal diffusivity in a reacted sample provides a measure of connectivity and porosity in the bulk sample, which can complement visual observation of a cross-section.

At the onset of the reaction, thermal diffusivity has a direct influence on ignition and wave propagation. In a high-density sample, it can be very difficult to ignite a reaction due to rapid diffusion of heat away from the region of the sample adjacent to the igniter. Eventually, the temperature near the igniter is high enough for the reaction to start, but the sample temperature is no longer uniform and the thermal influence of the igniter cannot be neglected. This is often the case for intermetallics, as the intrinsic thermal diffusivity of the elements is high [1] and the particles are soft, deforming during compaction to create good contact between the particles. An accurate knowledge of thermal diffusivity in the compact is therefore essential for a good understanding of the process.

It is difficult to estimate thermal diffusivity in porous solids, as the mean field theory is not stricto sensu valid for transport properties (*e.g.* thermal conductivity or diffusivity, electrical conductivity, and viscosity), although this rule yields acceptable results for low porosities [2] and for some fully dense composites. For extremely high porosities, it is easy to visualize the occurrence of percolation phenomena and therefore the invalidity of the rule of mixtures. However, for intermediate porosities, *i.e.* from 20 to 70%, transport properties depend on the pore distribution and morphology. For example, a porous copper sample made of long whiskers would have very different electrical and thermal conductivities than one composed of small platelets separated by pores: the former would look like an electrical wire, be very conductive, and be described by a parallel model (the resistances of pores and copper are parallel); the latter would be like a capacitor and be very resistive, best described by a serial model. Compacted powders present an intermediate case, with

[a] e-mail: vrel@limhp.univ-paris13.fr
[b] UPR 1311
[c] UMR 6630

porosity between 30 and 50%, and thus the two limiting cases present too large a discrepancy for their predictions to be satisfactory.

To model SHS, three coupled equations are used: heat diffusion, chemical kinetics and heat exchange with the surroundings. As these equations are coupled and highly non-linear, separating the influence of diffusivity from the effects of the reaction on thermal gradients is an almost impossible task. Most analyses – including the well-known Boddington model (see *e.g.* [3,4] for a complete description of the model and its use in the determination of activation energies) – are based on the assumption of a constant value for thermal diffusivity. This assumption has become so common that very few models consider the variation of thermal diffusivity as a function of temperature and/or composition. Measuring thermal diffusivity therefore becomes a key step to extend our understanding of such reactions.

On the other hand, measuring thermal diffusivity at high temperatures is not an easy task: the most common method, called the "flash method", requires that the sample be held at constant high temperature, such as in a high temperature homogeneous furnace. A pulse of heat is brought to one end of the sample and the diffusion of this additional heat is examined at the opposite end of the sample. The heat can be brought to the sample either by a homogeneous flat heating element (at low temperatures) or, more traditionally, following the early works of Parker in 1961 [5], by an impulse of light. Whereas the original system used a xenon flashlamp, modern systems usually use a powerful laser. For the method to be reliable, the sample must be quite small: the facing surface must be entirely and homogeneously exposed to the light, and the sample length must be small, so that the heat reaches the other end in a short time with negligible radial losses. This method has been adapted to very high temperatures [6] with the use of a periodic heat pulse, which participates in the sample's global heating, brought by a CO_2 laser. Thermal diffusivity is then determined by the phase difference between the heat source at one end of the sample and the measured temperature at the other. Measurements at temperatures up to 3000 K have been performed with such a system. Finally, a method has been proposed to measure thermal diffusivity in a thin layer [7], using infrared thermography to follow non homogeneous temperature profiles on the sample. Whereas the geometry and the problem described in this paper is quite different from ours, the methodology is similar.

All these methods require small, thin samples with parallel faces. In addition, measuring thermal diffusivities at high temperature is a long process. The initial temperature must be homogeneous, and an inert atmosphere (usually He) is required to prevent oxidation. The thermal characteristics of the atmosphere can influence the measurements, as porosity implies that heat may be transferred through the pores as well as the bulk. Nitrogen or argon is commonly used during SHS reactions. Moreover, as SHS reactions are so fast, the materials produced are often slightly inhomogeneous, and the measurement procedure described above can induce re-crystallization, sintering, grain growth, relaxation of internal composition gradients or destruction of possible transient phases. Thus, the measured value may not be representative of the real sample. Indeed, an attempt was made to use such an apparatus to measure thermal diffusivity of TiC produced *via* SHS as a function of temperature, from room temperature to 1600 °C and back to room temperature, but the curve with decreasing temperature was not consistent with the one with increasing temperature, suggesting that the microstructure of the sample was greatly modified by the measurement. At the end of the procedure, the sample's surface was covered with needle-like crystals, a strong indication of re-crystallization at high temperature. It is therefore desirable to find a method by which thermal diffusivity may be measured very quickly, in conditions as close as possible to the synthesis conditions. An attempt at such a method is presented here.

2 Experimental setup

Reactant powders consisted of commercial Ti and graphite powders. The mean diameter of the Ti particles, as measured by laser granulometry, was about 17 μm, while the mean diameter of the carbon particles was fairly coarse, about 22 μm. Stoechiometric proportions of Ti and C were weighed out and thoroughly mixed in a Turbula homogenizer for an hour. Compacts were formed in a stainless steel die with double-action rams and a load of 12 kN. The resulting sample was a cylinder 12.1 mm in diameter and about 15.2 mm in height. The sample's mass was 3.989 g, and the green relative density was 0.61.

The experimental system in which the combustion synthesis was performed has been fully described elsewhere [8]. The experimental chamber was evacuated and backfilled with high purity nitrogen at ambient pressure three times, then put under a constant nitrogen flow for about ten minutes at the same pressure. Ignition was provided by a graphite plate, $0.5 \times 5 \times 20$ mm, connected to a high current AC transformer (up to 12 V and 200 A). Less than 5 seconds after the connection of the graphite plate, the reaction started and propagated with an average velocity of about 1.7 mm s^{-1}. The reaction was studied using an infrared camera (AVIO TVS 2000 ST) with simultaneous Time Resolved X Ray Diffraction (TRXRD) using an X-ray synchrotron beam (H10 Beamline, LURE, Orsay, France). The sampling rate was 25 frames per second.

3 Experimental results

Figure 1 is a thermal image of the sample immediately after the combustion reaction, as recorded by the infrared camera. One can observe that the end of the sample reached extremely high temperatures, much higher than the maximum temperatures reached in the rest of the sample. This is a common occurrence in SHS, as conductive heat transfer is more efficient than convection or radiation. The heat that diffuses ahead of the reaction front

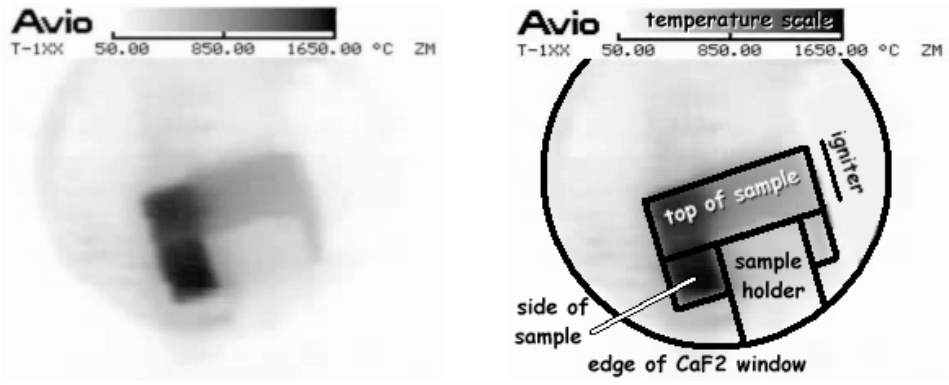

Fig. 1. Thermal image of the top surface of the sample, 0.4 s after the reaction front has reached the end of the sample. Right: schematic of the different parts of the image. The temperature scale (uncorrected for thermal emissivity) ranges from 50 °C (light) to 1650 °C (dark).

during the wave propagation reaches the end of the sample and cannot escape quickly, inducing an increase in temperature.

In the sample examined here, however, the thermal image shows a temperature difference of about 600 K between the two ends of the sample, much larger than is usually observed. Moreover, the temperature increase is quite abrupt: the last quarter of the sample is above 1300 °C while the first half of the sample is below 900 °C. The transition between these two regions is thus very narrow.

Figure 2 presents a streak image of the evolution of temperature with time for a line running the length of the sample, as indicated at the bottom of the figure. The image is 27 seconds long, beginning at the bottom of the image. First, a few points representing the hot graphite igniter are seen on the right, for about 5 seconds. The reaction then ignites, and a wave of heat travels to the left, ahead of the reaction propagation. The dark horizontal line near the top of the image marks the time at which the reference picture was taken (Fig. 1 and the bottom of Fig. 2), just after the reaction has reached the end of the sample. Figure 3 shows the evolution of temperature with time at four points along the sample. At each point, the first temperature peak represents the reaction wave, but the second unusually large peak remains to be explained. One explanation of Figure 3 is that the sample has undergone a first reaction, propagating from the igniter to the opposite end of the sample, and then a second reaction starting at the far end, triggered by an undetected phenomenon. Such an observation is very unlikely, but has been observed by other researchers [9]. An alternate explanation rests on the instability of the combustion wave. In Figure 2, it may be observed that initially, propagation is almost steady. After about 15 seconds, the propagation pauses and heat is transferred toward the end of the sample without reaction. After about five seconds, propagation accelerates again and extremely high temperatures are reached due to the heat built up during the pause. Consequently, the heat generated by the reaction diffuses to the rest of the sample, and different points along the sample axis experience two strong temperature increases, as shown in Figure 3. The first peak corresponds to the

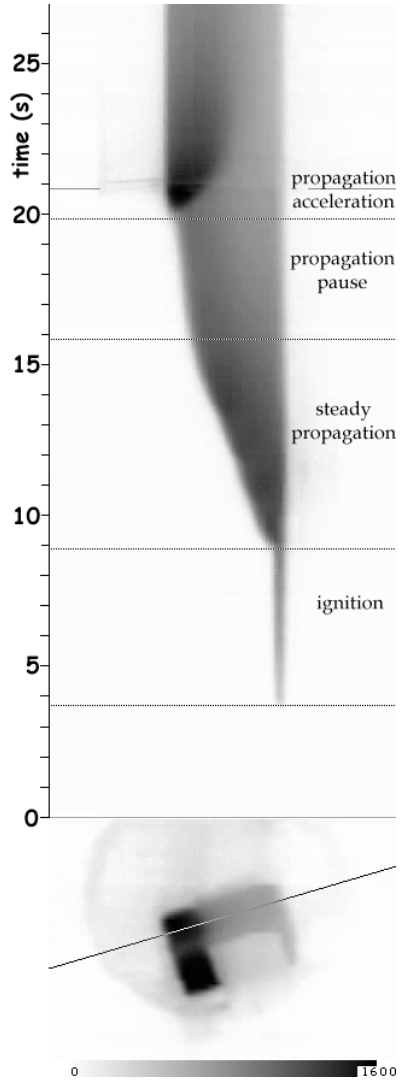

Fig. 2. Bottom: thermal image, similar to Figure 1. Top: thermal evolution as a function of time of the temperature profile along the line drawn across the sample in the bottom part.

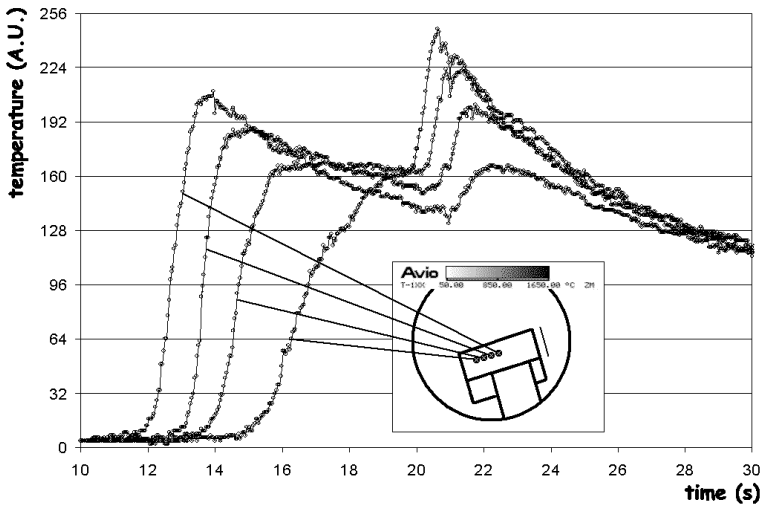

Fig. 3. Temperature profiles for 4 points along the propagation axis on the sample. Inset: location of the points on the surface of the sample.

reaction front itself, and the second peak to the back-diffusion of heat generated at the end of the sample.

Proof that a second reaction based on intermediate products is not occurring may be seen in Figure 4, TRXRD patterns recorded during the reaction. The horizontal axis represents the diffraction angle (2θ) and the vertical axis represents the time, for a total duration of 40.96 s. A more complete description of X ray diffraction on this sample will be published elsewhere [10]. At the bottom, the dark lines are the Ti and graphite peaks in the initial reactant mixture. When the reaction wave reaches the position of the X ray spot, a strong left shift (*i.e.* towards small angles) is seen, depicting the lattice parameter increase due to the large temperature increase. This shift is more pronounced and thus more easily observed in the higher angle diffraction peaks. All the Ti peaks then abruptly disappear, to be replaced by titanium carbide peaks, left shifted due to the combustion temperature. The sample then starts to cool, due to heat losses, but some 8 seconds later, an abrupt left shift is again observed corresponding to an increase of the lattice parameter due to re-heating. No change in the nature of the peaks is observed, as no reaction is taking place. The second temperature peak observed in Figure 3 is thus also observed in Figure 4. The time difference between heat peaks in Figure 4 ($\sim$8 s) agrees with the time difference between peaks of the second curve in Figure 3, suggesting that the location of this curve corresponds to the position of the X ray spot.

Finally, in contrast to the microstructures of many samples with spin instabilities, the structure of the sample is homogeneous, and no internal cracks, whose effect on thermal diffusivity would have been drastic, are observed.

To acquire temperature profiles from the thermal images captured after the reaction, a routine was written to rotate the image in Figure 1, 18 degrees clockwise, to obtain a horizontal rectangle. Each point after rotation is calculated from the weighted average of 4 initial points. In order to obtain a good one-dimensional temperature

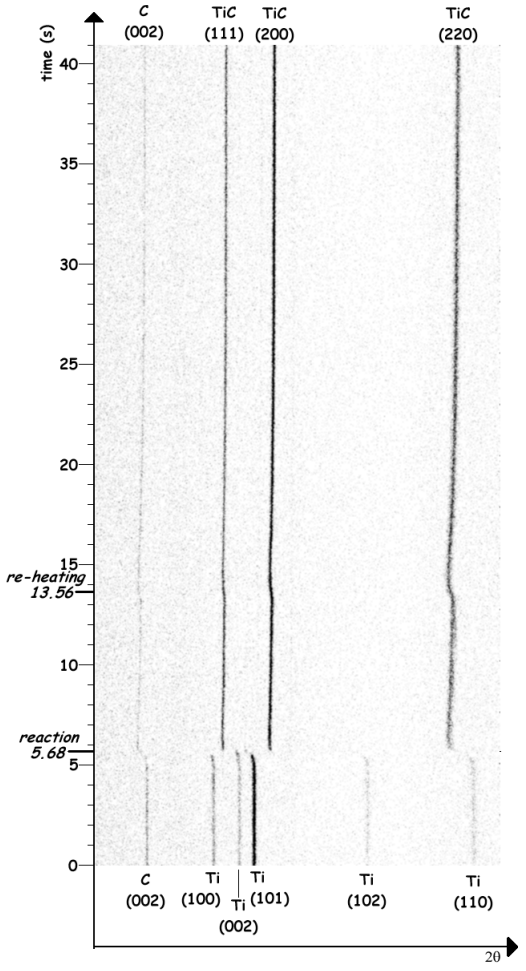

Fig. 4. Diffraction pattern of the sample during the reaction Ti + C $\rightarrow$ TiC. Horizontal axis: angle (2θ); vertical axis: time in seconds. Intensity of the diffraction lines is represented by the darkness of the points. The two time steps marked in italics indicate the time at which the reaction wave reaches the analysis point, and the time at which re-heating is observed at the same point.

profile, the intensities of all the points in each line of pixels perpendicular to the propagation direction are averaged, excluding 2 mm on each side of each line. Finally, the light intensity is converted to temperature. The conversion of the color thermal images to 256 gray levels has been described previously [8]. To obtain the temperature in kelvin, a correction must be made for the emissivity of TiC, reported to be 0.7, as the images were recorded using an emissivity of 1.0. To perform the conversion, a routine calculates the light flux received by the camera, then integrates the monochromatic emissivity as a function of the temperature in the detection range of the camera, 3 to 5.4 μm in wavelength. It then finds the temperature for which the same integration multiplied by 0.7 gives the same value for the light flux. The temperature of a point determined in this way is higher than the uncorrected temperature and can exceed 1650 °C.

4 Model

To calculate thermal diffusivity from the temperature profiles recorded after the reaction, a model was developed using two adjustable parameters: thermal diffusivity (α) and heat losses (ξ). Using an initial temperature profile, these two parameters are optimized to fit the temperature profile measured one second later.

Heat diffusion in a cylindrical solid can be described by the following equation:

$$\frac{\partial T}{\partial t} = \alpha \left[\frac{\partial^2 T}{\partial x^2} + \frac{1}{r} \frac{\partial}{\partial r} \left(r \frac{\partial T}{\partial r} \right) \right] \tag{1}$$

where T is the temperature, t the time, α the thermal diffusivity, and x and r are the axial and radial directions of the sample. Assuming a linear variation of the temperature in the radial direction allows equation (1) to be simplified to:

$$\frac{\partial T}{\partial t} = \alpha \left[\frac{\partial^2 T}{\partial x^2} + \frac{1}{r} \left(\frac{\partial T}{\partial r} \right) \right]. \tag{2}$$

At the sample surface, heat losses are mainly radiative, due to very high temperatures. Thus, radial heat losses may be described as follows:

$$-\lambda \frac{\partial T}{\partial r} = \varepsilon \, \sigma \left(T^4 - T_\infty^4 \right) \tag{3}$$

where λ is the thermal conductivity ($\mathrm{J\,s^{-1}\,K^{-1}\,m^{-1}}$), ε the emissivity (0.7) and σ the Stephan-Boltzmann constant (5.67×10^{-8} $\mathrm{W\,m^{-2}\,K^{-4}}$). Thus, combining equations (2, 3) leads to:

$$\frac{\partial T}{\partial t} = \alpha \frac{\partial^2 T}{\partial x^2} - \xi \, \varepsilon \, \sigma \left(T^4 - T_\infty^4 \right) \tag{4}$$

where $\xi = \frac{1}{\rho C_p r}$, ρ is the mass per unit volume and C_p is the heat capacity. In reacting powder compacts, ρ and C_p are not precisely known, and thus ξ is treated as an adjustable parameter. Equation (4) is then discretized using a one-dimensional, explicit numerical scheme, with 77 space steps (corresponding to the length of the image, 77 pixels) and a time step of 10^{-4} s:

$$T_{n+1}^i = T_n^i + \alpha \frac{\Delta t}{\Delta x^2} \left(T_n^{i+1} - 2T_n^i + T_n^{i-1} \right) - \frac{\xi}{\rho \, C_p \, r} . \varepsilon . \sigma \left(T_n^{i_4} - 298^4 \right) \Delta t \tag{5}$$

where T is temperature, the subscripts represent time, superscripts represent space, Δt is the time step, and Δx is the space step. The simulation runs very rapidly; for a given α and ξ, a temperature profile may be calculated in less than one second on a personal computer. The two parameters α and ξ are independently varied using the gold number-based dichotomy method (or *golden section search*, see *e.g.* [11]), a four-point method in which the function is calculated at only one point at each step, to minimize the sum of the square of the differences between the calculated and measured profiles after 1s. Details are presented in Table 1. The gold number method decreases the uncertainty of the parameter under consideration by a factor of about $0.618 (= \frac{\sqrt{5}-1}{2})$ at each step. 50 steps were performed, reducing the initial interval to 3.55×10^{-11} times the original value. The initial intervals were $[0{:}10^{-3}]$ for α and [0:1] for ξ. The method is therefore mathematically extremely precise, although the final result is accurate only if the model can accurately describe the observed phenomenon. The temperature values for the first and last space step in the model (boundary conditions) were calculated by a linear time interpolation between the initial and final measured temperatures for the corresponding pixels:

$$\begin{cases} T_t^0 = (1-t) \; T_{t=0}^0 + t \; T_{t=1}^0 \quad (0 < t < 1) \\ T_t^{77} = (1-t) \; T_{t=0}^{77} + t \; T_{t=1}^{77} \; (0 < t < 1). \end{cases} \tag{6}$$

An interval of one second for each simulation, rather than 1/25th second, the time between two thermal images, was chosen to increase the temperature change between the two profiles being compared, and thus to reduce the effect of noise in the profiles. Between two neighboring profiles, the change in temperature is small and thus scatter in the measured temperature can have a larger effect than if the change in temperature is large.

In summary, the simulation proceeds as follows:

1. The temperature profile at a given time is acquired from a thermal image. For convenience, call this time $t = 0$.
2. Using an estimate for α and ξ selected by the gold number method (Tab. 1), the discretized heat transfer equation is used to calculate a temperature profile one second later, at $t = 1$.
3. The difference between the measured temperature profile and the calculated profile (both at $t = 1$) is calculated as the sum of the squares of the differences between points.
4. Another estimate for ξ is made by the gold number method, and steps 2 and 3 are followed again.

Table 1. Algorithm for the gold number dichotomy method for the optimization of α. Note that for each value of α, ξ is optimized using the same process so that each temperature profile is calculated using an optimized value of ξ for that particular value of α.

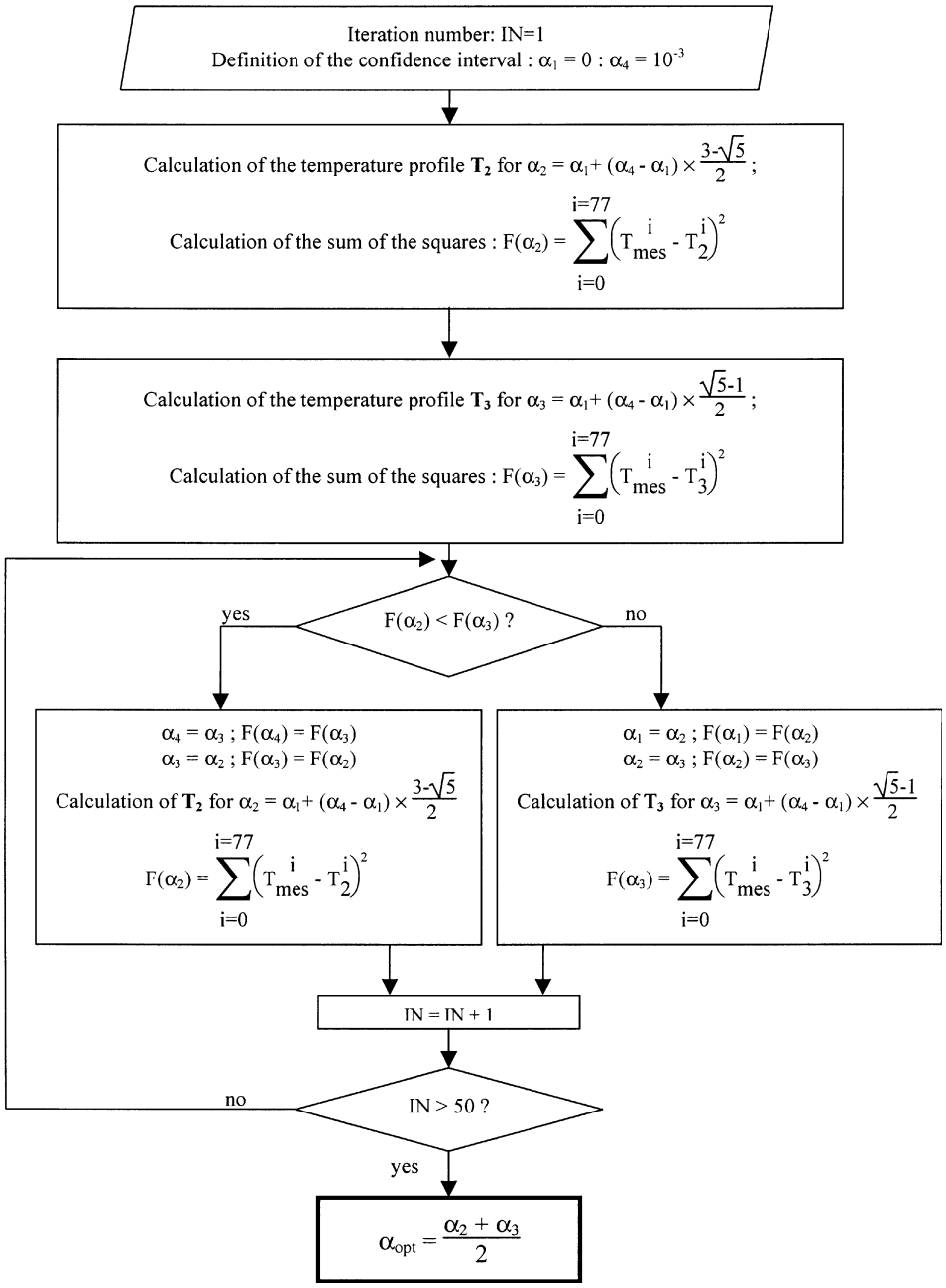

5. This procedure is repeated 50 times, the number of iterations chosen for the gold number method.
6. Another estimate for α is made by the gold number method, and steps 2, 3, 4 and 5 are followed again.
7. This procedure is repeated 50 times, the number of iterations chosen for the gold number method.
8. The best values for α and ξ, as well as the final difference from the measured profile at $t = 1$ (the error), are plotted in Figure 5 at each $t = 0$.
9. The next thermal image, 1/25 second later, is used as a new $t = 0$ and the process is repeated from step 1.

5 Discussion

Figure 5 presents the best values for α and ξ and the associated error calculated for each thermal image as a function of simulation start time: the horizontal coordinate is the time (measured from the end of the reaction) of the initial temperature profile used for each simulation ($t = 0$, see above). As the first point in Figure 5 shows, the result of the simulation initiated 0.2 s after the end of the reaction deviates strongly from the measured profile. In addition, ξ converges to 0, the smallest allowable value,

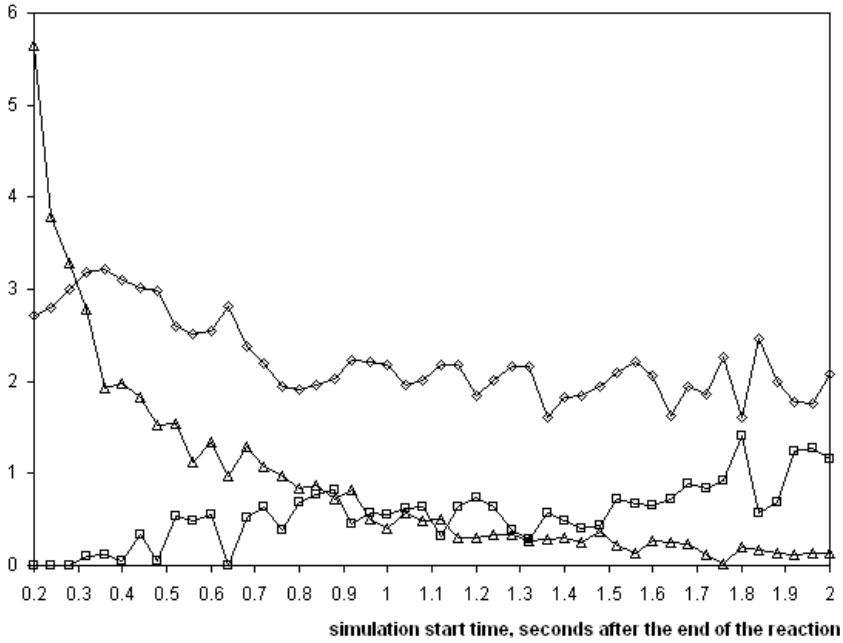

Fig. 5. Results of the model. The model is performed for 1 second, *i.e.* 25 frames, the number of the first frame being represented as the horizontal axis: points at 0.2 s are the results of the simulation performed between 0.2 s and 1.2 s. ◊: optimized value for α, $\times 10^6$; □: optimized value for ξ, $\times 10^3$; and △: sum of the squares between calculated and measured values of temperature, $\sum_i (T_{calc} - T_{mes})^2$, $\div 3 \times 10^4$.

in the first few simulations. If the allowable interval of ξ is set to include negative values, *e.g.* $[-1{:}1]$, the gold number optimisation converges to a negative value. A negative value for heat losses has no physical meaning, and it is also extremely unlikely that heat losses would be zero at the hottest time after the reaction, as suggested by a value of zero for ξ. One can therefore conclude that this analysis is not accurate for a time period of about 0.5 s after the end of the reaction, most likely because the internal temperature gradients are not uniform immediately after the reaction, particularly at the end of the sample that has just reacted. After the initial 0.5 s, the temperature has become more uniform across the width of the sample, the one-dimensional model becomes more accurate, and the error between the calculated and measured temperature profiles becomes smaller and smaller.

Unfortunately, as the difference between the calculated and measured profiles grows smaller, so does the temperature gradient along the length of the sample, increasing the uncertainty in α. This uncertainty may be seen in Figure 5, as the values for both α and ξ vary more at later times. For this reason, the final values for α and ξ are taken to be the average of all values calculated from 0.72 s to 2 s after the end of the reaction, 33 values in all. For α, the value is 2.00×10^{-6} m^2 s^{-1} with a standard deviation of 0.20×10^{-6} (10%). This value is about 4 times the value measured previously at low temperatures [12,13]. Although this is a large change, theoretical work on thermal conductivity in porous and highly porous materials [14–17] predicts such an evolution with temperature. Applying the law for thermal diffusivity temperature dependency described in [14], one reaches the value of 1.85×10^{-6} m^2 s^{-1} from these low temperature measurements [12], in excellent agreement with current measurement. Moreover, the thermal profile analysis performed using the Boddington model [18] allows us to estimate an average thermal diffusivity of (1.5 ± 0.6) 10^{-6} m^2 s^{-1} on the same material [10]. In contrast, the linear rule of mixtures yields a value around 9.6×10^{-6} m^2 s^{-1}, more than four times too high.

For ξ, an average of 7.0×10^{-4} m^2 K J^{-1} is calculated, with a standard deviation of 2.7×10^{-5}, 5%. This value is about three times higher than a reasonable estimate for $1/\rho C_p r$, 2×10^{-4}, indicating that heat losses are under-estimated by only taking into account radiative heat losses. As a result, ξ must be assumed to include more terms than solely $1/\rho C_p r$.

Figure 6a presents detailed results for the simulation performed starting at 0.72 s after the end of the reaction and ending at 1.2 s after the reaction, when the deviation of the simulation from the measured temperature profile is largest. This large error is not very large in the context of the profiles, as the simulated profile (solid line) is qualitatively similar to the measured profile (open squares). This simulated profile was obtained by calculating forward one second from the initial measured profile (open diamonds). Comparing the initial and final measured profiles, we see that the temperature near the hot end of the sample (the end farthest from the ignition source) has fallen rapidly in one second. At about the thirty-second pixel, the final temperature exceeds the initial temperature, indicating heat transfer from the hot end toward the cold end. However, at the very end of the sample, the final temperature is again below the initial temperature, evidence that

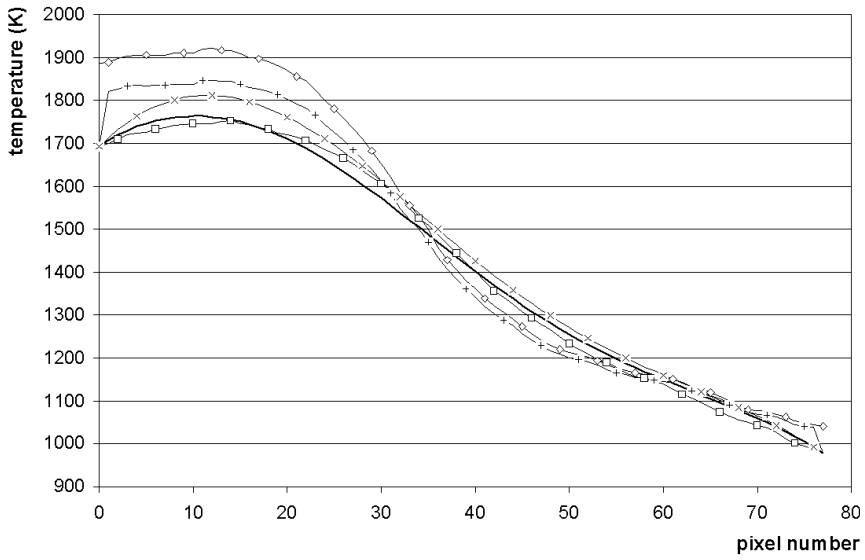

(a)

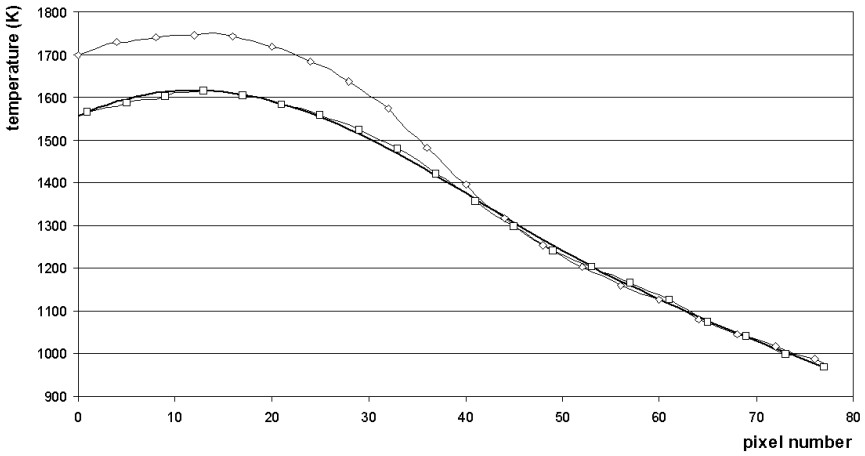

(b)

Fig. 6. Spatial temperature profile. ◊: initial measured temperature profile; □ final measured temperature profile, 1 second later; continuous line: calculated temperature with optimized values for α and ξ, x: calculated temperature profile with α optimized and ξ set to 0; and +: calculated temperature with ξ optimized and α set to 0. a) Profiles for 0.72 s and 1.72 s, b) Profiles for 1.76 s and 2.76 s.

either heat diffusion has not yet reached this point or that losses are greater at this point.

The other two curves in Figure 6a ($\times$ and $+$) represent the results of the same model, first when α is optimized and ξ is set to 0 and then *vice versa*, to determine the contribution of each parameter. The curve in which α is set to 0 (heat losses only) runs below and almost parallel to the initial temperature profile, except for the boundary pixels, which are set to the final measured values. In contrast, the curve in which ξ is set to 0 follows the final temperature profile fairly closely, including the diffusion of heat from the hot end to the center of the sample but not all the way to the cold end. This suggests that thermal diffusivity is more important to the thermal behavior of the sample than heat losses are. However, if the temperature gradient were not so steep, or the overall temperature lower, losses might become more important.

Figure 6b presents the measured temperature profiles at 1.76 s and 2.76 s as well as the calculated profile at 2.76 s; all three are much closer together than the profiles in Figure 6a. The values for α, ξ, and the error for this simulation are plotted in Figure 5 at 1.76 s.

An attempt was made to find α as a function of temperature by plotting α *vs.* the average temperature in each simulation. However, the average profile temperature varied significantly from the norm only in the first points, from 0.2 s to 0.7 s, points that were previously discarded due to large errors. Considering the points from 0.7 s onward, this technique is not sensitive enough to discern any variation in α with temperature in the present

temperature range. An attempt was also made to perform a two-parameter optimization for α, considering a cubic dependency on temperature, to take into account the influence of radiative heat transfer through the pores: $\alpha = \alpha_0 + \alpha' T^3$, but the fit was not improved and α' always converged to 0. Thus it seems the temperature dependency of α is screened by the noise in the data.

Some other refinements could be made to the model, such as the inclusion of convective heat losses or variation of emissivity (ε) as a function of temperature. These modifications yield only a slight variation in the error, too slight to justify the introduction of another semi-arbitrary parameter. The boundary conditions could be modified such that rather than assuming a linear change from one temperature to the temperature one second later, the values for the end pixels from each of the 23 intermediate temperature profiles could be used. However, since the time step is 10^{-4} s, adjusting the boundary conditions 23 times out of 10,000 steps would not add sufficient accuracy to be worthwhile.

Unfortunately, this method requires a fairly steep temperature gradient when no reaction is occurring, a condition which is not often present after steady-state wave propagation. A slight temperature increase at the end of the reaction has often been noted, and it may be possible to use this increase to calculate α. It may also be possible to use a laser to provide pulsed heat input in the same manner as traditional thermal diffusivity measurements, but *in situ*, to the great advantage of metastable product phases.

6 Conclusions

A method has been developed to calculate high-temperature *in situ* thermal diffusivity in combustion-synthesized materials immediately after the combustion reaction, using only an infrared camera and a computer model. This method offers the advantages of short experiment time and direct measurement of a property that has been measurable only in conditions far from those present during a combustion reaction. These advantages should prove important for metastable materials. The rapidity and convenience of the measurement should assist in the understanding of the effects of different powder compact parameters on the reaction, as it may be performed for each sample reacted.

The value obtained for the thermal diffusivity of TiC at temperatures between 1000 and 1900 K, 2.00×10^{-6} m^2 s^{-1}, is about four times larger than values measured at room temperature [12], and agrees well with estimations deduced from the Boddington model [18] and with theoretical predictions for the behavior of thermal diffusivity in porous materials at high temperatures.

The authors would like to express their gratitude to M. Gailhanou, and D. Thiaudière, from the Lure facility, for their help during the TRXRD experiments. Ellen M. Heian and Nikhil Karnatak wish to thank, respectively, the French Ministry of Research (Direction de la Recherche) and the Région Poitou-Charentes for financial support.

References

1. T. Akiyama, H. Isogai, J.-I. Yagi, AIChE J. **44**, 3, 695 (1998)
2. A.A.A. Zenin, A.G. Merzhanov, G.A. Nersisyan, *Thermal wave structure in SHS processes (by the example of boride synthesis)*, English translation of Fisika Goreniya y Vzryva **17**, 1, 79 (1981)
3. M.-C. Dumez, R.-M. Marin-Ayral, J.-C. Tédenac, J. Alloys Compounds **268**, 141 (1998) and references within for Boddington's original works
4. R.-M. Marin-Ayral, M.C. Dumez, J.-C. Tédenac, Mater. Res. Bull. **35**, 233 (2000)
5. W.J. Parker, R.J. Jenkins, C.P. Butler, G.L. Abbott, Flash J. Appl. Phys. **32**, 1679 (1961)
6. M. Laurent, H. Helali, C. Fort, High Temperatures-High Pressures **26**, 317 (1994)
7. I. Philippi, J.C. Batsale, D. Maillet, A. Degiovanni, Rev. Sci. Instrument **66**, 182 (1995)
8. D. Vrel, N. Girodon-Boulandet *et al.*, Rev. Sci. Instr. **73**, 422 (2002)
9. J.H. Lee, A.Y. Lee, C.C. Chen, J. Mater. Res. **13**, 1626 (1998)
10. N. Karnatak, S. Dubois, M.F. Beaufort, D. Vrel, *Kinetic and mechanisms of titanium carbide formation by SHS using time resolved X-Ray diffraction and infrared thermography*, to be published
11. W.H. Press, S.A. Teukolsky, W.T. Vetterling, B.P. Flannery, *Numerical Recipes in C*, 2nd edn. (Cambridge University Press, 1992), Chap. 10
12. D. Vrel, Ph.D. thesis, *Synthèse de matériaux céramiques par combustion auto-entretenue de poudres (procédé SHS). Modélisation et application au carbure de titane*, June 27, 1995 (in French), Paris XIII University
13. D. Vrel, Sci. Theor. J. Super-hard Mater. **111**, 3 (1998)
14. B. Schulz, High Temperatures-High Pressures **13**, 649 (1981)
15. A.V. Luikov, A.G. Shashkov, L.L. Vasiliev, Yu.E. Fraiman, J. Heat Mass Transfer **11**, 117 (1968)
16. G. Flamant, J.D. Lu, B. Viarot, Trans. ASME **116**, 652 (1994)
17. K. Nasr, R. Viskanta, S. Ramadhyani, Trans. ASME, J. Heat Transfer **116**, 829 (1994)
18. T. Boddington, P.G. Laye, J.R.G. Pude, J. Tipping, Combustion Flame **47**, 235 (1982)